Moroccan Journal of Chemistry
ISSN : 2351-812X

Mor. J. Chem., 2024, Volume 12, Issue 4, Page 1664-1682
https://revues.imist.ma/index.php/morjchem
https://doi.org/10.48317/IMIST.PRSM/morjchem-v12i4.51347

Study of Reactive blue 203 removal by TiO_2-P25 adsorption combined with photocatalysis for its degradation

Fatima Zaaboul[1,*], Chaimae Haoufazane[2], Asmae Kari [1], Rajae Salim[3], Kkalil Azzaoui[3,4*], Rachid Sabbahi[3,5], Abderrahim El Hourch[1*]

[1]*Laboratory of Materials, Nanotechnology and Environment, Faculty of Sciences, Mohammed V University in Rabat, P.O. Box. 1014, Rabat, Morocco*
[2]*Plant Chemistry and Organic and Bioorganic Synthesis Team, Faculty of Sciences, Mohammed V University in Rabat, P.O. Box. 1014, Rabat, Morocco*
[3]*Euromed University of Fes, UEMF, Fes, Morocco*
[4]*Engineering Laboratory of Organometallic, Molecular Materials and Environment, Faculty of Sciences, Sidi Mohammed Ben Abdellah University, 30000 Fez, Morocco*
[5] *Research Team in Science and Technology, Higher School of Technology, Ibn Zohr University, Laayoune, Morocco.*

**For Corresponding authors: zaaboul.fatima00@gmail.com (F. Zaaboul), k.azzaoui@yahoo.com (K. Azzaoui)*

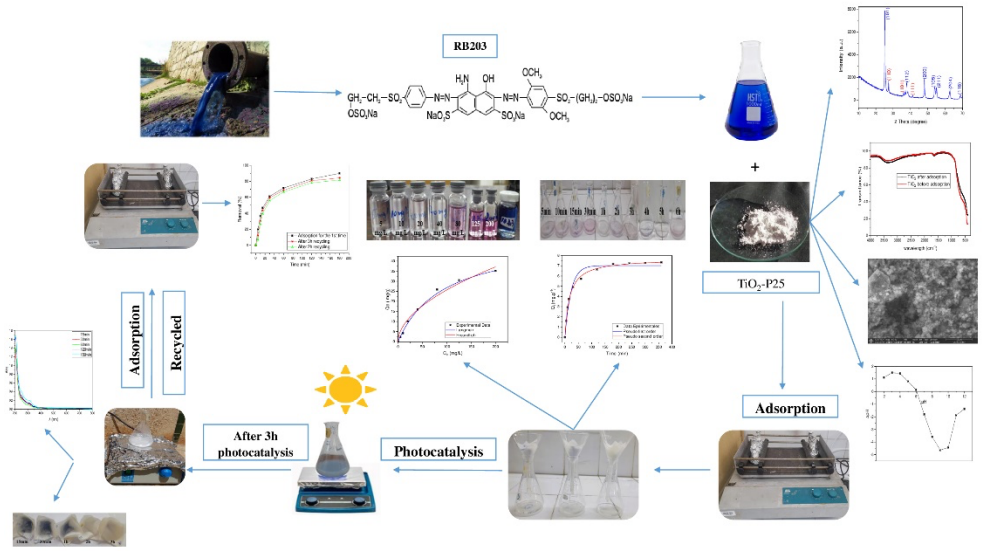

Received *18 May 2024,*
Revised *14 Sept 2024,*
Accepted *16 Sept 2024*

Citation*: Zaaboul F., Kari A. Salim R., Azzaoui K., Sabbahi R., El Hourch A. (2024) Study of Reactive blue 203 removal by TiO_2-P25 adsorption combined with photocatalysis for its degradation, Mor. J. Chem., 12(4), 1664-1682*

Abstract: The treatment of wastewater containing textile dyes is a major environmental challenge due to the complexity of the effluents and the diversity of chemical compounds involved. In this study, we explored adsorption and photocatalysis to improve the purification efficiency of these waters. Adsorption on TiO_2-P25 proved particularly effective in removing Reactive blue 203 (RB-203) dye, reaching equilibrium in around 180 min with optimum conditions —a 25mL volume containing 40 mg/L dye, 0.125 g TiO_2-P25, pH 3, stirring speed 300 rpm, and temperature 25 °C. Photocatalysis using TiO_2-P25 has shown promising results under solar irradiation, particularly with TiO_2-P25 recycling techniques to reduce costs and improve durability. This study proposes effective solutions for the treatment of wastewater containing textile dyes, with specific recommendations for their practical application in industrial facilities, and future prospects include the optimization of treatment conditions and the integration of these processes into wider systems for sustainable environmental management.

Keywords: *TiO_2; RB-203; Solar photocatalysis; Photodegradation; Adsorption, Water treatment.*

1. Introduction

Since ancient times, textile dyes have played a crucial role in human cultures, providing the means to dye fabrics and express cultural identity through clothing (Wozniak *et al.* 2023; Mourid *et al.,* 2021). The first natural dyes, extracted from plants, animals, and minerals, were gradually replaced by synthetic dyes from the 19th century onward. The invention of the first synthetic dye, mauveine, by William Henry Perkin in 1856 marked the start of an industrial revolution in textile dye production (Ihmels 2019). These synthetic dyes offered a wider range of colors and greater durability than natural dyes. However, the rise of synthetic dyes has also had significant environmental consequences (El Abdouni *et al.* 2021).

Wastewater from the textile industry often contains dye residues that are difficult to break down and can be toxic to aquatic flora and fauna (Dutta *et al.* 2024, Bouammali *et al.*, 2024). These dyes can cause problems such as eutrophication of water bodies, disruption of aquatic ecosystems, and risks to human health in the event of contamination of drinking water sources. Today, several processes for purifying and reducing organic pollutants have been developed to significantly improve the selectivity and efficiency of contaminant removal techniques (Tkaczyk *et al.* 2020, Tabaghtet al. 2023). These include coagulation/flocculation, membrane filtration, and chemical and biological treatments. However, adsorption onto porous solids remains one of the most used techniques (Hasanpour *et al.* 2020). Indeed, conventional adsorbents are in great demand due to their high adsorption capacity and large specific surface area, but the performance and efficiency of this adsorption technique depend predominantly on the nature of the support used as an adsorbent, its cost, abundance, and regeneration (Burakov *et al.* 2018). At the same time, advanced oxidation processes (AOPs) are gaining in popularity for their ability to effectively degrade recalcitrant organic compounds present in wastewater (El-Hafed *et al.* 2024, Azzaoui et al. 2017, Saidi et al. 2022).

AOPs are based on the generation of highly reactive hydroxyl radicals ($^{\cdot}OH$), which attack and break down dye molecules into less harmful or completely mineralized products (Assila *et al.* 2021, Azzaoui et al. 2015). The main types of AOP include chemical oxidation (such as the Fenton process, photo-Fenton, and ozonation) and photocatalysis (often utilizing TiO_2) (Ajmal *et al.* 2018, Azzaoui et al. 2016). These technologies offer significant advantages, including complete degradation of pollutants without producing toxic secondary residues (Ammari *et al.* 2016, Akartasse et al. 2022, Hamed et al. 2019). However, they require investment in infrastructure and energy, which can make their operating costs high compared with conventional methods. The aim of this work is to compare and evaluate the effectiveness of two distinct methods for the removal of textile dyes from wastewater: adsorption of a textile dye "Reactive Bleu 203 (RB-203)" on TiO_2-P25 and photocatalysis using TiO_2-P25 as a semiconductor.

The present work aims to study the solar photocatalytic degradation of an organic pollutant such as reactive blue 49 and to compare two TiO_2 (P25) catalysts (Giwa *et al.* 2012). The catalysts were characterized by various analytical techniques, including X-ray diffraction (XRD), infrared analysis (FTIR), and scanning electron microscopy (SEM). We also studied adsorption kinetics and photocatalytic degradation. Its adsorption activity after photocatalytic degradation was assessed by monitoring the transformation of RB-203 taken as a model organic pollutant.

2. Methodology

2.1 . Material

Evonik's TiO_2-P25 is composed of around 70% anatase and 30% rutile, with a minor amorphous phase. It has a specific surface area of 55 ± 15 m^2/g and a particle size of around 30 nm. Sodium hydroxide (NaOH, 99.0%) was supplied by VWR Prolabo Chemicals. Sulfuric acid (H_2SO_4, 96.0%) was supplied by Panreac.

2.2 Reactive Colorant Blue 203

2.3 Adsorbent characterization: TiO_2-P25

TiO2 was fully characterized, including structural, morphological and optical analyses. The crystalline phase of TiO_2 nanoparticles was determined by powder X-ray diffraction (XRD) with a Shimadzu XDR-6100 instrument, using Cu K radiation (λ = 1.5406 Å). To identify the functional groups, present in TiO_2-P25, Fourier transform infrared spectroscopy (FTIR) analysis was carried out in the 4000-400 cm-1 range using a Bruker Alpha Platinum-ATR spectrometer with a KBr disk. TiO2 morphology was observed by Scanning Electron Microscopy (SEM) coupled to X-ray Energy Dispersion Spectrometry (EDS) using a Quanta 200 instrument. In addition, an analysis of the surface properties of TiO_2 was carried out to determine the pH_Z of this material using a pH meter from HANNA instruments.

We used Reactive Blue 203 (RB-203), also known by its trade name Remazol Marine Blue, which belongs to the azo dye family. Its chemical structure is illustrated in **Figure 1,** and its chemical characteristics are listed in **Table 1**.

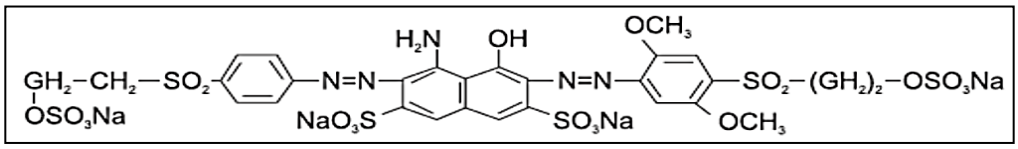

Figure 1. Chemical structure of RB-203

Table 1. Chemical characteristics of the dyes used.

Colorant	Formula	Molar mass (g/mol)	Solubility in water	λ_{max} (nm)
Reactive blue 203	$C_{28}H_{29}N_5O_{21}S_6.4Na$	1051,87	High	605

2.4 Description of adsorption tests

All experiments were carried out using the stock solution of initial dye concentration 40 mg/L (0.01 g) prepared in a 250 mL flask. In an Erlenmeyer flask, 0.125 g TiO_2 and 25 mL dye were mixed. The adsorbent/adsorbate mixture is then stirred at room temperature (25 °C) for 3 h at a speed of 300 rpm on an orbital shaker**,** and the solution is filtered through filter paper (Table 2).

2.5 Analysis method

After filtration, UV-visible spectrophotometric analysis was carried out to determine the impact of the various effects on absorption at a wavelength of 605 nm. Next, the adsorption capacity (Q_{Ads}) in (mg/g) and the removal rate (R%) were calculated according to the following equations (Kannan *et al.* 2022, Azzaoui et al. 2014):

$$Q_{Ads} = \frac{(C_0 - C_e).V}{m} \quad (1)$$

$$R(\%) = \frac{(C_0 - C_e)}{C_0} \times 100 \quad (2)$$

where C_0: initial concentration in mg/L, C_e: equilibrium concentration in mg/L, **V**: volume of dye solution in mL, and m: mass of adsorbent in g.

Table 2. Summary of effects studied, their fixed and varied parameters for adsorption.

Effects Studied	Fixed Parameters	Varied Parameters
Contact time	Initial concentration: 40 mg/L Volume: 25 mL Adsorbent mass: 0.125 g	Time in min: 5, 10, 15, 30, 60, 120, 180, 240, 300, 360
Adsorbent mass	Initial concentration: 40 mg/L Volume: 25 mL Time: 180 min	Adsorbent mass in g: 0.0125, 0.025, 0.075, 0.175, 0.225, 0.275, 0.325
Initial pH	Initial concentration: 40 mg/L Volume: 25 mL Adsorbent mass: 0.125 g Time: 180 min	pH: 3, 5, 6.63, 9, 11, 12
Adsorbate concentration	Volume: 25 mL Adsorbent mass: 0.125 g Time: 180 min	Solution concentration in mg/L: 5, 10, 20, 40, 80, 125, 200

2.6 Photolysis

A beaker containing 80 mL of the stock solution was placed on a magnetic stirrer and subjected to solar irradiation. Samples of 10 mL were taken at regular intervals of 10, 15, 30, 60, 120, and 180 min. Then, 2 mL of each sample taken was analyzed using a UV-visible spectrophotometer to determine its concentration from the measured absorbance.

2.7 Photocatalysis

After adsorption of RB-203 dye by TiO_2-P25 by modifying several factors influencing adsorption, the dye-saturated TiO_2–P25 powder obtained after filtration of adsorption solutions carried out under fixed conditions (40 mg/L dye, 0.125 g TiO_2, 25 mL bidistilled water, dye pH, 3 h) was recovered to degrade the dye present on the adsorbent surface by photocatalysis (Figure 2). Five Erlenmeyer flasks were prepared, each containing 0.25 g dye-saturated TiO2-P25 and 25 mL bidistilled water. The Erlenmeyer flasks were exposed to sunlight under magnetic stirring, and the stopwatch was started. The duration of photocatalytic degradation varied from 15 to 180 min (15, 30, 60, 120, and 180 min). The solutions were then filtered using filter paper, and samples were taken and analyzed using a UV-visible spectrophotometer. Solar photocatalytic degradation experiments were carried out under similar conditions on sunny days between 11 a.m. and 2 p.m. in May 2024.

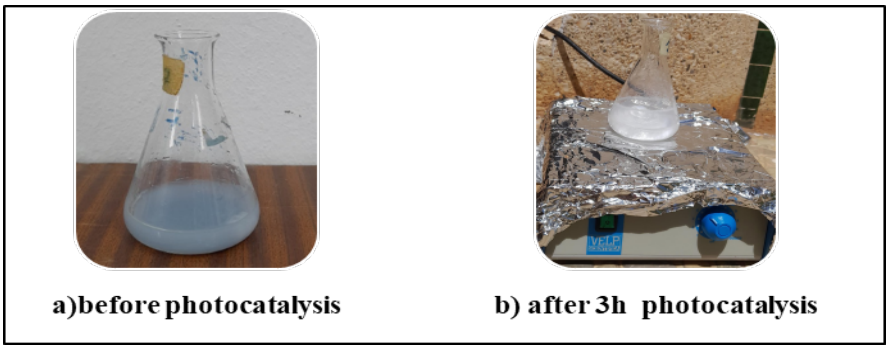

Figure 2. Aqueous solution before and after three hours of photocatalysis.

3. Results and Discussion

3.1 Adsorbent characterization

3.1.1. Mineralogical analysis by XRD

Figure 3 shows the DRX diagram of Degussa TiO_2-P25, which is a mixture of 80% anatase and 20% rutile. Notable peaks in a range of $10° < 2\theta < 70°$ were observed for anatase at 25.21°, 37.81°, 47.96°, 53.91°, 54.97°, 62.66°, and 68.85°, corresponding to the following Miller index (hkl) values: (101), (112), (200), (105), (211), (204), and (116), respectively, and for rutile, three peaks were observed at 27.43°, 36.06° and 41.20° corresponding to the Miller (hkl) index values: (110), (101), and (111), respectively (Al-Taweel *et al.* 2016). The diffraction peaks are all well indexed to the pure anatase phase according to JCPDS standard map no. 99-101-0679. This has been validated by similar results from several published works (Srinivasan *et al.* 2019).

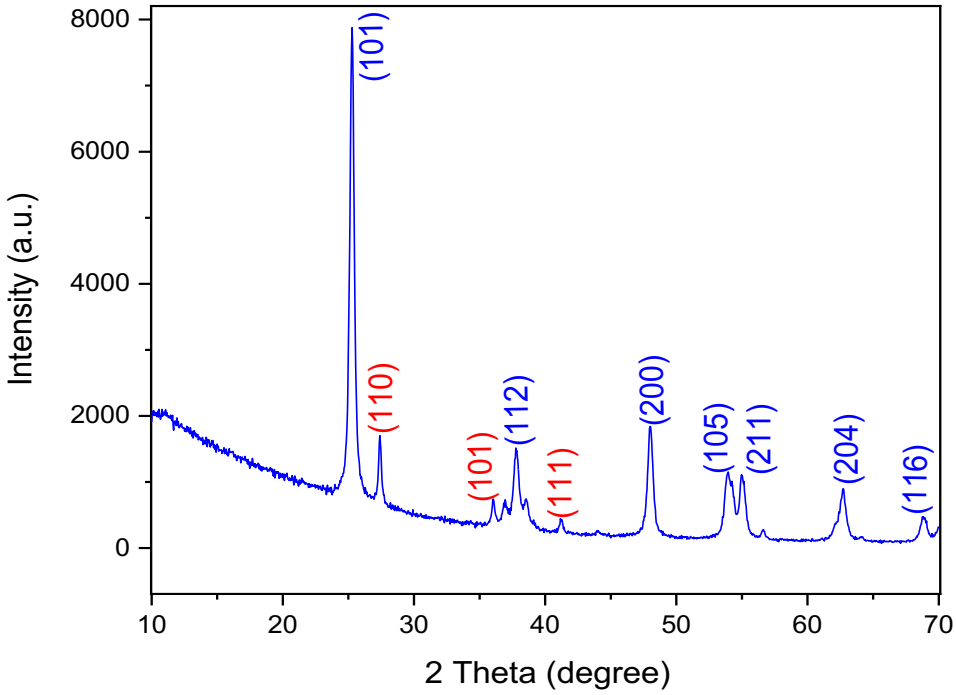

Figure 3. X-ray diffractogram of TiO_2 - P25

3.1.2. Analysis by FTIR

Figure 4 shows the FTIR spectrum of TiO_2-25 before and after adsorption of RB-203 dye. The main absorption bands are between 500 and 750 cm^{-1}, 1627 cm^{-1}, and a broad band between 3107 and 3593 cm^{-1}. The band between 500 and 750 cm^{-1} can be attributed to the stretching vibration of the Ti-O and Ti-O-Ti bonds within the TiO_2-25 structure; this band indicates the presence of chemical bonds in the material and is crucial for characterizing the TiO_2-25 structure **(**Vetrivel *et al.* 2015**)**. The band at 1627 cm^{-1} corresponds to the characteristic vibration band of the O-H group. The presence of this hydroxyl group is important as it indicates interaction with water or other compounds containing hydroxyl groups. This may have significant implications in various TiO2 applications, including its reactivity with water or its ability to adsorb compounds containing hydroxyl groups. The band between 3107 and 3593 cm^{-1} corresponds to the intermolecular interaction between the TiO_2 surface and the hydroxyl group of water molecules. This interaction is crucial in many TiO_2 applications, particularly in heterogeneous catalysis and photocatalysis, where water is often present as a reagent. Analysis of this

band can provide insights into the nature of the interaction between TiO_2 and water, which is essential for understanding the reaction mechanisms involved in these processes (Nasiruddin and Sawar, 2007).

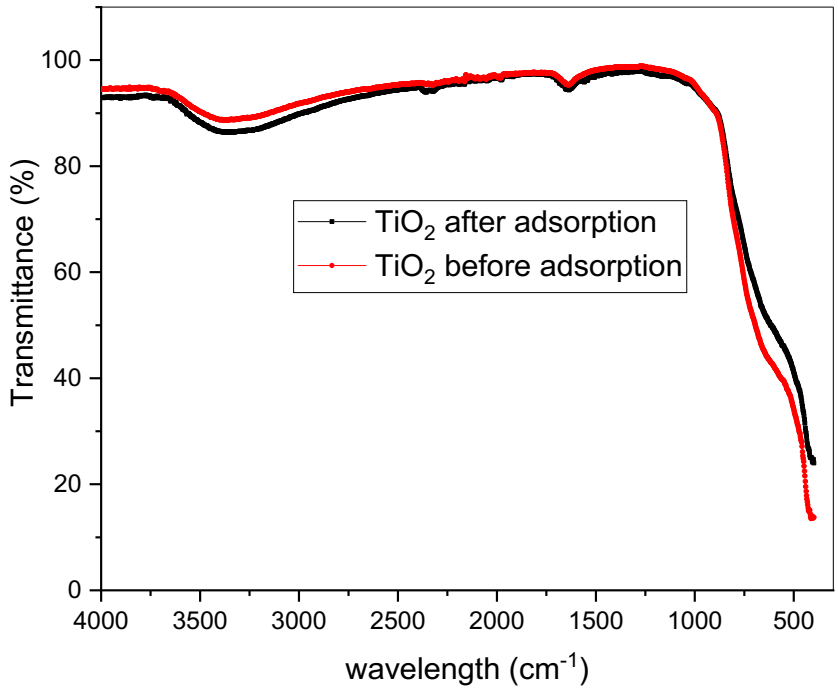

Figure 4. FTIR spectrum of TiO_2-P25 before and after adsorption

3.1.3. Morphological analysis by SEM/EDS

Analysis by scanning electron microscopy (SEM) and energy dispersive spectroscopy (EDS) provides valuable information on the morphology and elemental composition of the sample. SEM images of the TiO_2-P25 sample (**Figure 5**) show a surface formed of agglomerated nanoparticles, characteristic of titanium dioxide (TiO_2), with an irregular, heterogeneous texture (Annan *et al.* 2021). EDS analysis confirms a predominance of titanium (Ti) and oxygen (O), the main constituents of TiO_2, with mass proportions of 59.6% for titanium and 40.4% for oxygen. These results are in line with the expected composition of TiO_2-P25, widely used in photocatalysis due to its specific properties. The notable absence of contaminants testifies to the high purity of the sample (Moreira *et al.* 2018).

3.1.4. Determination of the pHpzc of TiO_2-P25

Figure 6 shows the determination of the point of zero charge (pHzc) for the TiO_2-P25 catalyst, which is equal to 6.1. The pH_pzc is the point at which the catalyst surface has no net charge, meaning that the amount of positive and negative charge is balanced at the catalyst surface (Kosmulski 2016).

- **pH < pHpzc:** When the pH is below 6.1, the TiO_2 surface becomes positive due to the protonation of hydroxyl groups (Ti-OH) present on the surface. The following chemical reaction takes place:

$$Ti - OH + H^+ \rightarrow TiOH_2^+ \quad \textbf{(3)}$$

- **pH > pHpzc:** When pH exceeds 6.1, the TiO_2 surface becomes negative due to deprotonation of hydroxyl groups. The corresponding chemical reaction is:

$$Ti - OH + OH^- \rightarrow TiO^- + H_2O \quad \textbf{(4)}$$

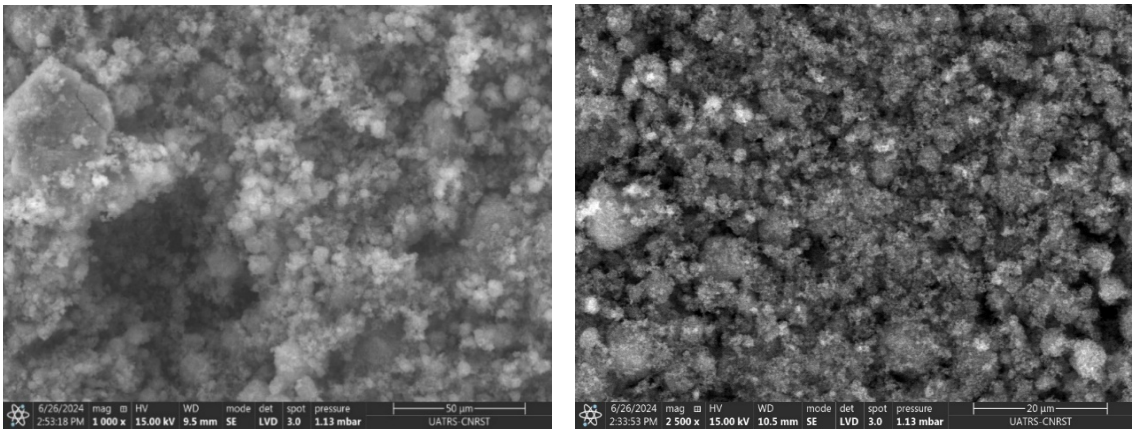

Figure 5. TiO_2-P25 morphology (a) and EDS composition (b).

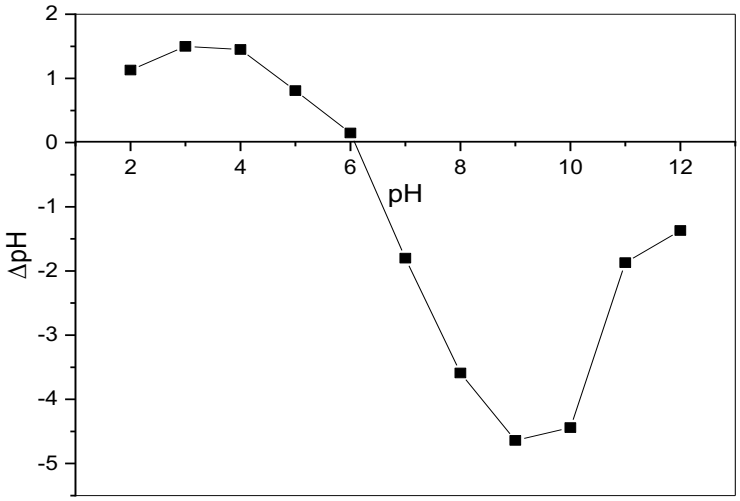

Figure 6. Determining the pHpzc zero charge point of TiO_2-P25

3.2 Removal of RB-203 by adsorption

3.2.1. Adsorbent mass effect

Figure 7 shows the evolution of RB-203 removal rate as a function of TiO_2-P25 adsorbent concentration (Jafari *et al.* 2015). The percentage removal of dye RB-203 increases with increasing TiO_2 concentration, reaching a plateau at 7 g/L (i.e. 0.175 g of TiO_2). The maximum elimination rate (87%)

is reached at a concentration of 7 g/L TiO2. This increase is attributed to the increase in sorption surface area and the availability of many active sites on the adsorbent. Above 7 g/L, the removal rate remains virtually unchanged, as the additional addition of TiO_2 no longer increases the free surface area of the grains due to the formation of agglomerates.

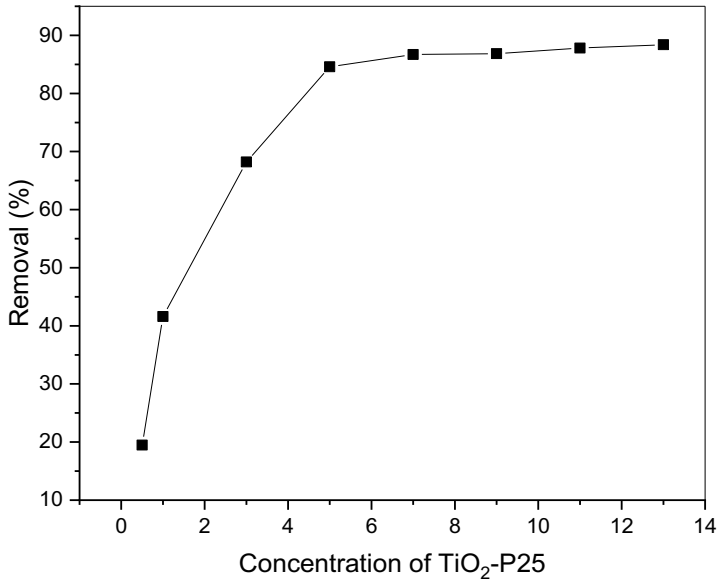

Figure 7. Evolution of the quantity of RB-203 adsorbed as a function of TiO_2-P25 concentration (C = 40 mg/L, t = 180 min, V = 25 mL, pH = 6.63, and ω = 300 rpm)

Figure 8 clearly shows the disappearance of the blue color from TiO_2-25 concentration equal to 7 g/L.

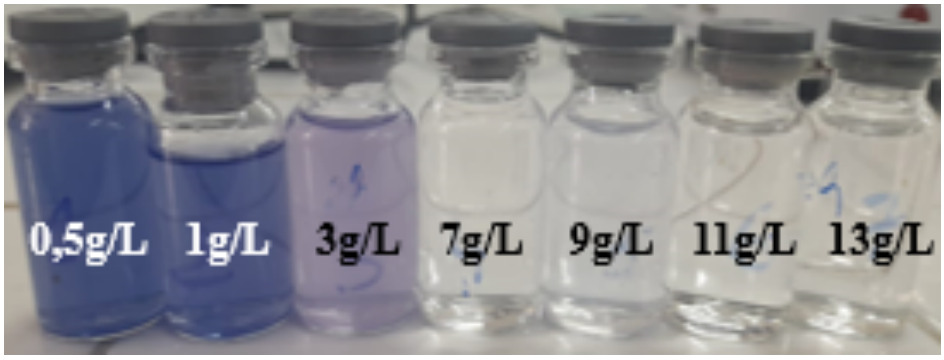

Figure 8. Solution samples prepared for the mass effect after 3 h adsorption on TiO_2-P25

3.1.2. Effect of initial pH

The pH of the solution is an essential parameter to be considered in the adsorption process, as it can affect both the charge on the adsorbent surface and the degree of ionization of the species in solution. It therefore controls the adsorption phenomenon (Mészáros *et al.* 2004) (**Figure 9**). The results obtained, illustrated in Figure 10, show that adsorption of RB-203 dye onto TiO_2-P25 is strongly influenced by solution pH. At acidic pH, adsorption of the dye is favored, particularly at pH = 3, where the removal rate is maximal (92%). At basic pH, dye adsorption is unfavorable, with removal rates dropping to 21% at pH = 12. Consequently, to maximize the adsorption of RB-203 on TiO_2-P25, it is preferable to work under acidic pH conditions. Figure 10 shows the color difference between solution samples prepared after 3 h adsorption on TiO_2-P25.

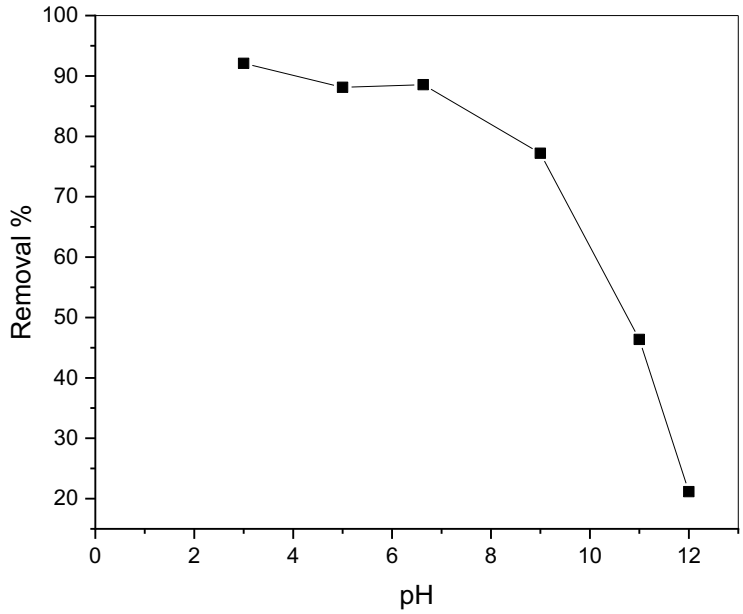

Figure 9. Evolution of the quantity of RB-203 adsorbed as a function of pH (C = 40 mg/L, m = 0.125 g, t = 180 min, V = 25 mL, and ω = 300 rpm)

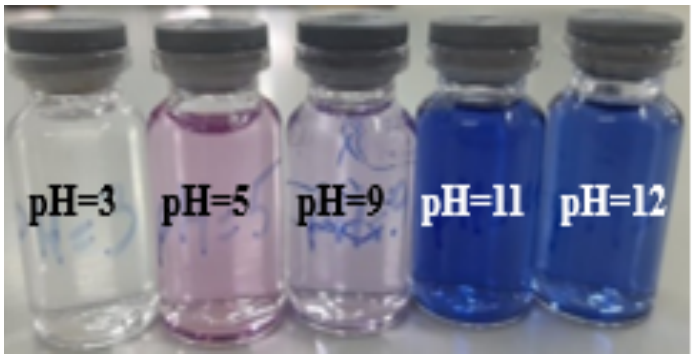

Figure 10. Samples of solutions prepared for the pH effect after 3 h adsorption on TiO_2-P25

3.2.3. Effect of contact time

Figure 11 shows the evolution of the removal rate of dye RB-203 as a function of contact time. The result shows a considerable increase in the removal rate as a function of time (Karim *et al.* 2009). We note that adsorption takes place rapidly during the first 60 min, with an elimination rate equal to 71.58%. This is since initially all surface sites of the adsorbent are available, but over time, adsorption efficiency decreases due to saturation of the active sites. The adsorption process takes place in two phases. The first phase is fast, due to the rapid attachment of RB-203 molecules to the TiO_2-P25 surface, and the second phase is slow, with a noticeable stabilization of the removal rate from 180 min, corresponding to a slower attachment leading to a state of equilibrium.

3.2.4. Adsorption kinetics of RB-203

Adsorption kinetic models enable us to study the equilibrium behavior of the dye RB-203 and to gather information on the reactions involved in adsorption (Elmoubarki *et al.* 2015)). Various models are proposed in the literature to describe adsorption kinetics, including first- and second-order kinetic models (Lima *et al.* 2020). The graphical representation and parameters of these two kinetic models are shown in **Figure 13** and **Table 3**. **Figure 12** visually illustrates how adsorption of RB-203 by TiO_2-P25 progresses with time, showing a reduction in solution color as adsorption becomes more efficient.

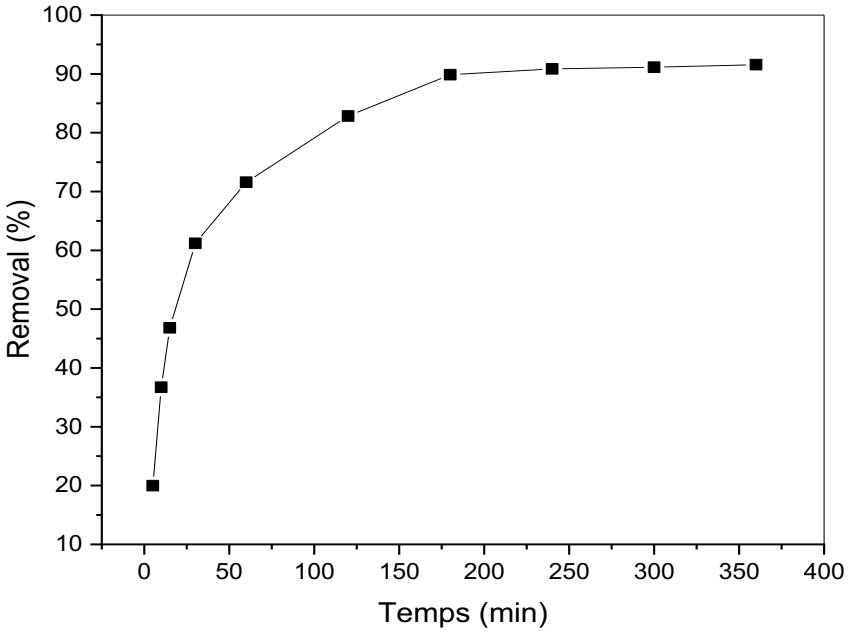

Figure 11. Evolution of the quantity of RB-203 adsorbed as a function of contact time (C = 40 mg/L, m = 0.125 g, V = 25 mL, pH = 6.63, and ω = 300 rpm)

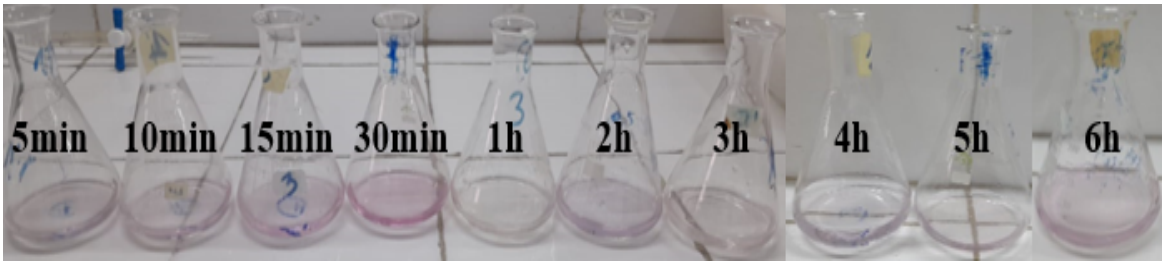

Figure 12. Samples of solutions prepared for the time effect

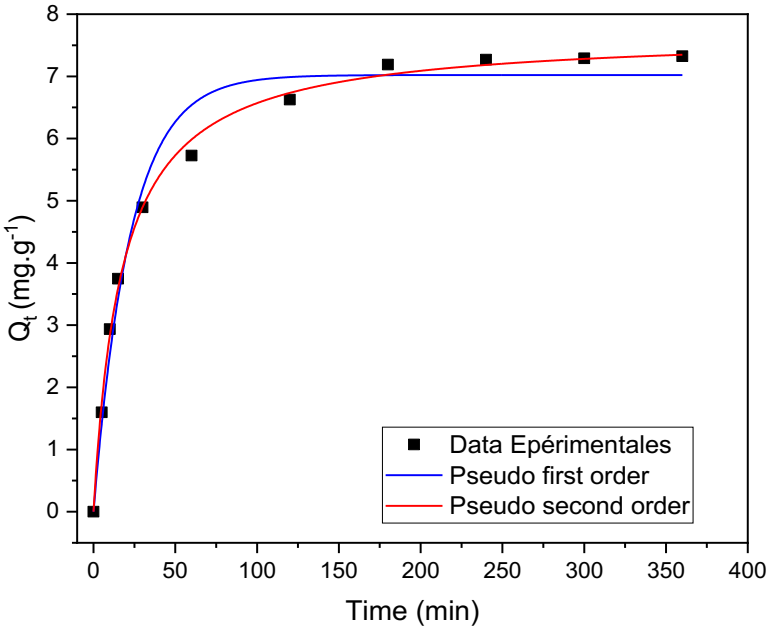

Figure 13. Plots of pseudo-first- and second-order kinetic model (m = 0.125 g, t = 180 min, V = 25 mL, pH = 6.63, and ω = 300 rpm)

Table 3. Pseudo first- and second-order kinetic model parameters

Model	Parameter	Value
Pseudo first order	Q_e (exp) (mg/g)	7.32489
	Q_e (cal) (mg/g)	7.69785
	K_1 (min^{-1})	0.04468
	R^2	0.97833
	SSE	18784.42404
Pseudo second-order	Q_e (exp) (mg/g)	7.32489
	Q_e (cal) (mg/g)	7.02157
	K_2 (g.min/mg)	0.00757
	R^2	0.99748
	SSE	109.44664

Observations in **Figure 13** show that the dye adsorbs rapidly onto the TiO_2-P25 surface during the first 30 min, explaining the adsorption potential of TiO_2-P25, then a plateau is observed at 180 min, indicating equilibrium, which could be due to the fact that dye molecules have occupied some adsorption sites; consequently, a decrease in adsorption sites or remaining color in solution was observed around 360 min. From the parameters in **Table 3** and the graphical representation of the kinetic model shown in **Figure 13**, it is evident that the adsorption process of dye RB-203 is well described by the pseudo-second-order model, as indicated by the high correlation coefficient (R^2 = 0.99748). additionally, the experimental Q_e value (7.32489 mg/g) is very close to the calculated Q_e value (7.02157 mg/g). These results suggest that the pseudo-second-order kinetic model is the main determinant of RB-203 adsorption on TiO_2-P25, as well as a lower SSE.

3.1.5. Effect of adsorbate concentration

The effect of the initial adsorbate concentration on the amount adsorbed is shown in **Figure 14.** It shows that the amount of RB-203 adsorbed by TiO_2-P25 increases with the initial dye concentration (Kordouli *et al.* 2015). This increase indicates that saturation has not yet been reached and that TiO_2-P25 can still adsorb larger quantities of RB-203 dye.

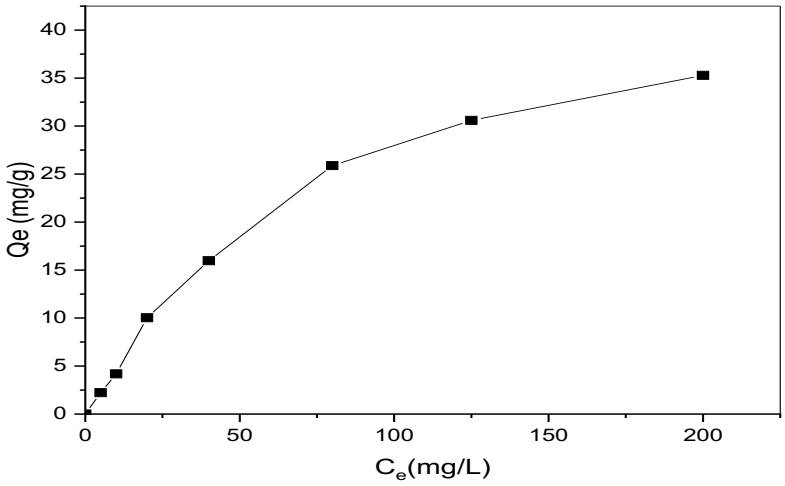

Figure 14. Influence of the initial concentration of RB-203 on the quantity fixed at equilibrium (m = 0.125 g, t = 180 min, V = 25 mL, pH = 6.63, and ω = 300 rpm)

Figure 15 clearly shows the disappearance of the blue color in concentrations below 40 mg/L of dye, which is the suitable concentration for a mass of TiO_2-P25 equal to 0.125 g.

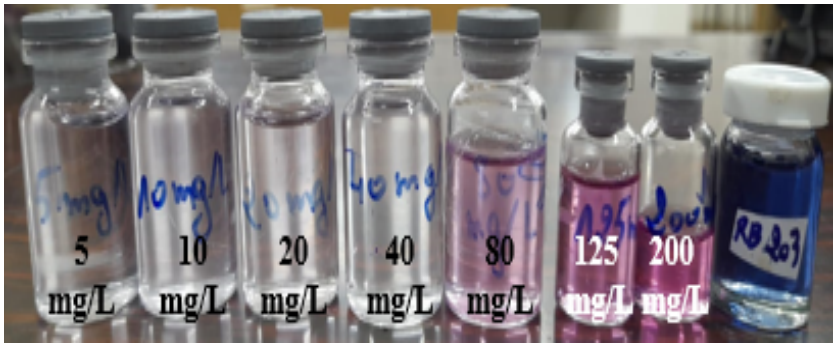

Figure 15. Solution samples prepared for the concentration effect after 3 h adsorption on TiO_2-P25

3.2.6 Adsorption isotherm for RB-203

Adsorption isotherms are important for the description of an interaction between adsorbate molecules and the adsorbent surface (Liu 2015). For the analysis of our results, we used Langmuir and Freundlich isotherms. Application of these two isotherms leads to the results shown in **Figure 16** and the adsorption parameters given in **Table 4**.

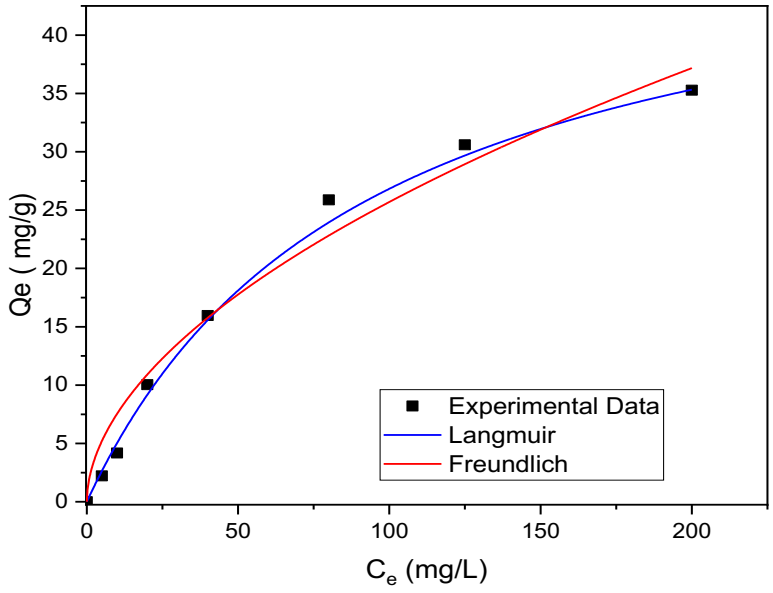

Figure 16. Langmuir and Freundlich modeling of experimental results (m = 0.125 g, t = 180 min, V = 25 mL, pH = 6.63, and ω = 300 rpm)

Table 4. Langmuir and Freundlich isotherm parameters

Isotherm	Parameter	Value
Langmuir	Q_m (mg/g)	51.70769
	K_L (L/mg)	0.01078
	R^2	0.99459
	SSE	58.94323
Freundlich	K_F (mg/g)	2.21212
	1/n	0.53254
	R^2	0.98559
	SSE	236.85118

To determine which model best describes the adsorption phenomenon under study, the value of the constant separation factor (K_L) was calculated to be 0.69. This indicates that the adsorption of RB-203 by the adsorbent is favorable according to the Langmuir model. Adsorption is better described by the Langmuir model (R^2 = 0.99459) and (SSE = 58.94323) than by the Freundlich model (R^2 = 0.98559) and (SSE = 236.85118), according to the data in **Figure 16** and **Table 4**, and by comparing the R^2 of the two models represented, which means that adsorption sites are uniform and finite, and adsorption is always monolayer. In addition, the Langmuir separation factor values lie between 0 and 1, within the range of validity. Langmuir's model assumes that entities adsorbed on similar sites do not interact. The results show that the Langmuir isotherm is the most appropriate to describe the adsorption of RB-203 by TiO2-P25.

3.3. Degradation of RB-203 by photolysis

Figure 17 shows the degradation kinetics of RB-203 by direct photolysis in an aqueous solution under solar irradiation (Halim *et al.* 2021). After 180 min (3 h) of irradiation, 14.47% of the dye had been degraded. This result shows that this molecule is difficult to degrade by direct photolysis under solar irradiation.

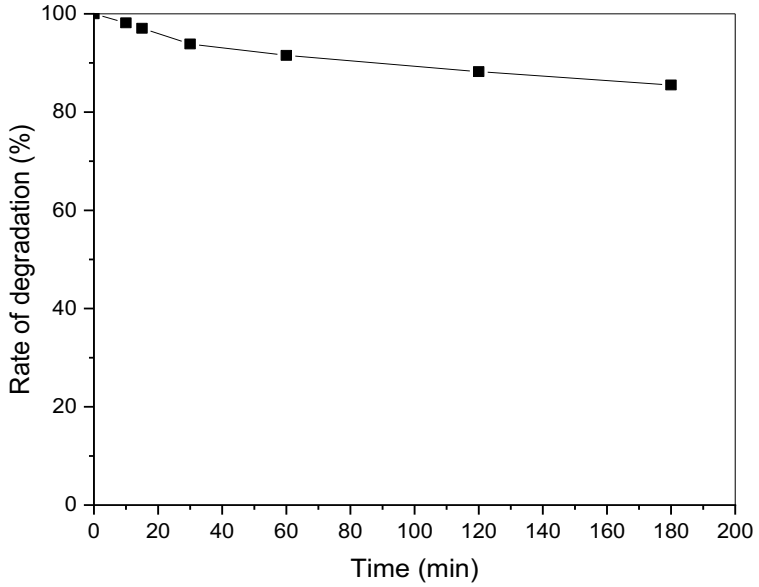

Figure 17. Degradation kinetics of RB-203 by direct photolysis in aqueous solution under solar irradiation

Figure 18 shows the samples taken during the photolysis experiment. At first glance, there appears to be no observable color degradation in the samples.

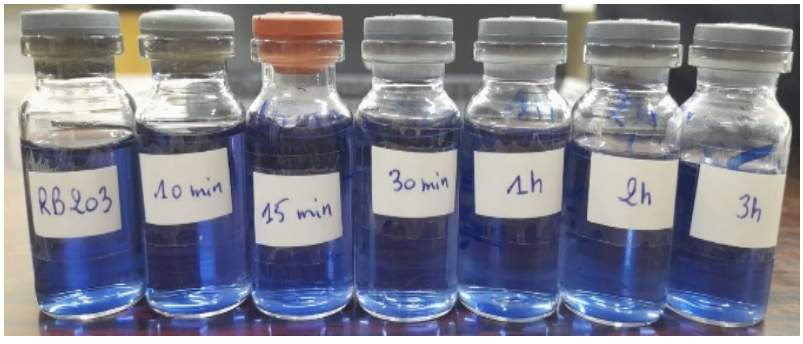

Figure 18. Samples taken during the photolysis experiment

3.4. Photocatalytic degradation of RB-203

After adsorption, sorbents saturated with harmful substances are usually disposed of directly into the environment, which can lead to major ecological problems (Moyé *et al.* 2017*).* Solving this problem requires practical, cost-effective regeneration of used sorbents, aimed at optimally improving the sorbent material and restoring its original absorption properties for subsequent reuse. To this end, this section aims to identify an effective and appropriate technique for depolluting TiO_2-P25 after its use in the RB-203 dye adsorption process, with the aim of combating environmental contamination and regenerating quantities of this adsorbent for future reuse. To achieve this, we applied the photocatalysis process.

3.4.1. Kinetics of RB-203 degradation by photocatalysis

Figure 19 shows a series of filter papers used to evaluate the efficiency of TiO_2-P25 photocatalysis on RB-203 dye degradation at different time intervals (15, 30, 60, 120, and 180 min) (Hu *et al.* 2020). Each filter reveals dark-colored deposits corresponding to dye and TiO_2-P25 residues. There is a progressive decrease in the intensity of coloration of the deposits on the filters, indicating increasing dye degradation over time. Notably, the last filter, marked (180 min), shows no coloration at all, demonstrating complete dye degradation after 3 h of photocatalytic treatment.

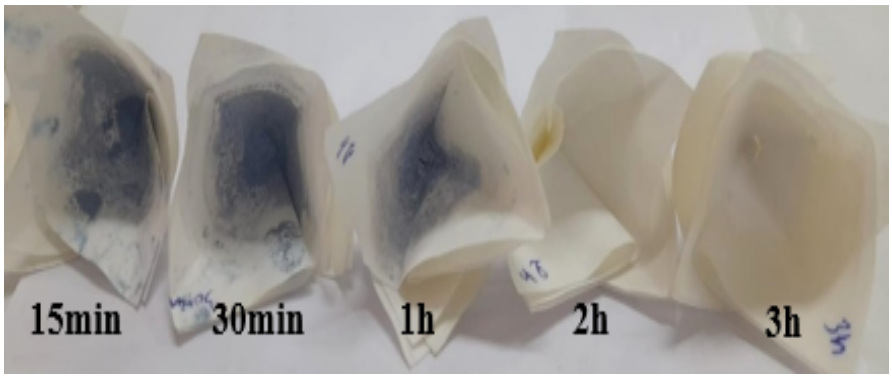

Figure 19. Changes in filter paper color after photocatalysis

3.4.2. Testing the purity of water samples after photocatalysis

To check that water samples taken after photocatalysis were not contaminated with TiO_2-P25, a test was carried out using UV-visible spectrometry. Each sample was analyzed for the presence of suspended TiO_2-P25 particles. The absence of characteristic TiO_2-P25 peaks (**Figure 20**) in the UV-visible spectra (**Figure 21**) confirmed that the water samples were free from photocatalyst contamination, thus ensuring the purity of the treated water.

3.4.3 Study of adsorption of RB-203 dye by recycled TiO_2-P25 after photocatalysis

Adsorption of RB-203 dye by recycled TiO_2-P25 after 2 and 3 h photocatalysis cycles was studied to assess the reuse efficiency of the photocatalyst. After each photocatalysis cycle, TiO_2-P25 was recovered and used to adsorb the dye in an aqueous solution. The results in **Figure 22** show that TiO_2-P25 retains a significant adsorption capacity after several photocatalysis cycles, although the efficiency may decrease slightly due to saturation of the active sites. In general, TiO_2-P25 recycled after 3h and after 2 h of photocatalysis shows a slightly lower adsorption efficiency compared to that used for the first time, with a decrease in percentage removal from 89.87% to 84.10% for 3 h photocatalysis and to 81.57% for 2 h. These results highlight the potential for reuse of TiO_2-P25 as an effective photocatalyst for organic dye removal.

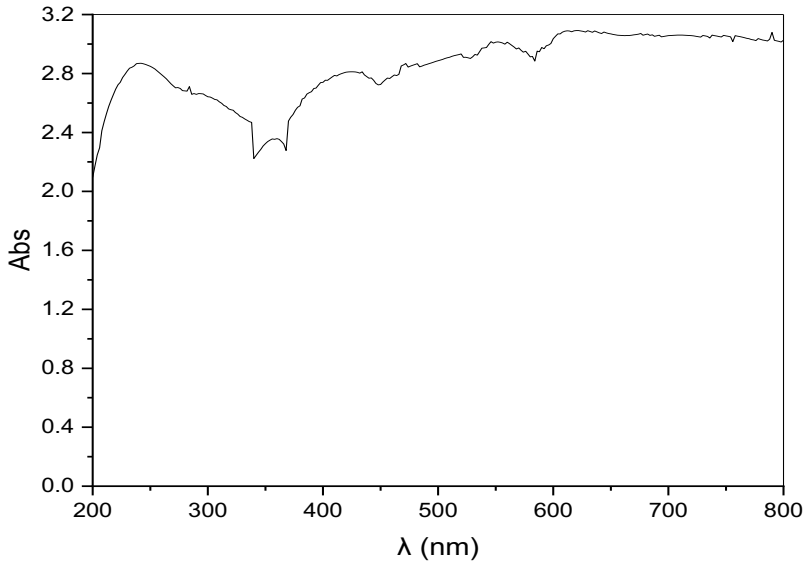

Figure 20. UV-visible absorption spectrum of TiO_2-P25 in solution

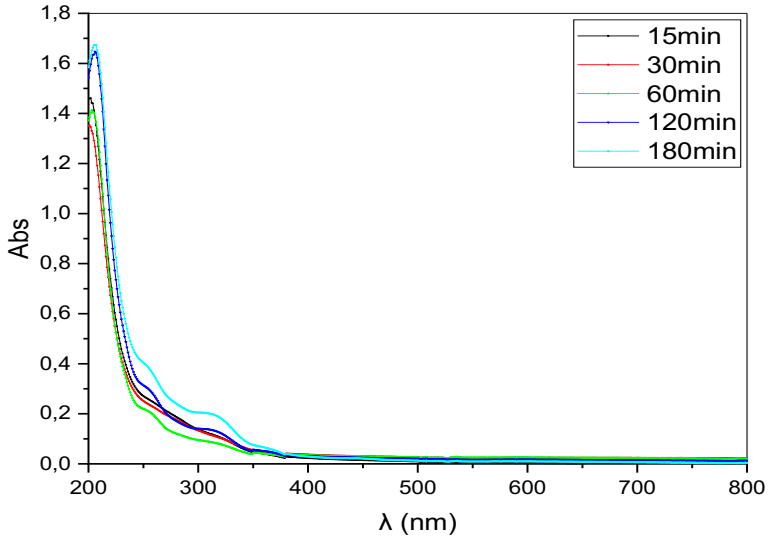

Figure 21. UV-visible spectra of water samples after photocatalytic treatment

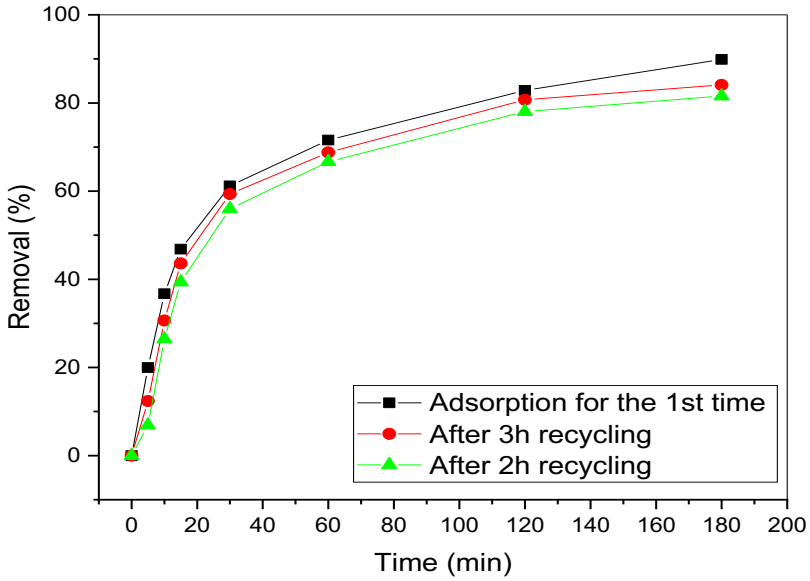

Figure 22. Evolution of adsorption removal rate of RB-203 dye after recycled TiO_2-P25 after 2 and 3 h photocatalysis

Figure 23 illustrates the filtration results of adsorption solutions using recycled TiO_2-P25 after photocatalysis times of 2 and 3 h. The filters show the distribution and intensity of residues after adsorption, with more intense coloration indicating greater retention of adsorbed particles.

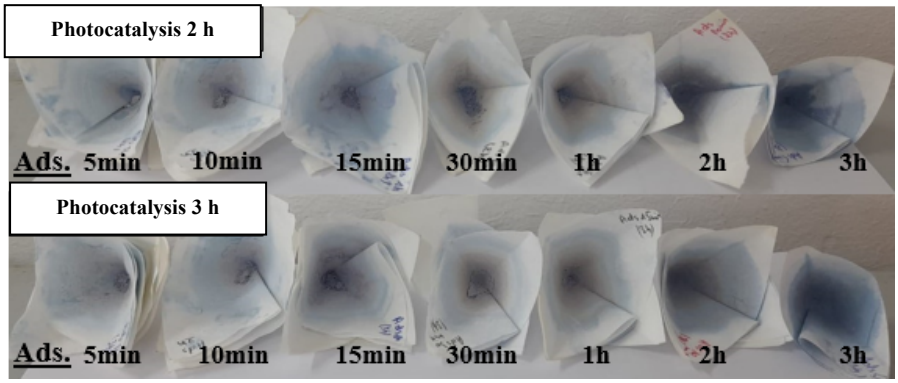

Figure 23. Evolution of filter paper coloration after adsorption of RB-203 by recycled TiO_2-P25 after 2 and 3 h photocatalysis

3.4.5. Degradation of RB-203 by direct photocatalysis

Figure 24 shows the degradation kinetics of RB-203 by direct photocatalysis in aqueous solution under solar irradiation (Jallouli *et al.* 2016). The result shows a considerable increase in degradation rate as a function of time. We note that dye degradation occurs rapidly during the first 5 min, with a degradation rate equal to 67.60%. Degradation then becomes slow over time, with a slight increase in the rate of degradation, followed by notable stabilization from 60 min to 180 min (3 h), reaching 98.77%.

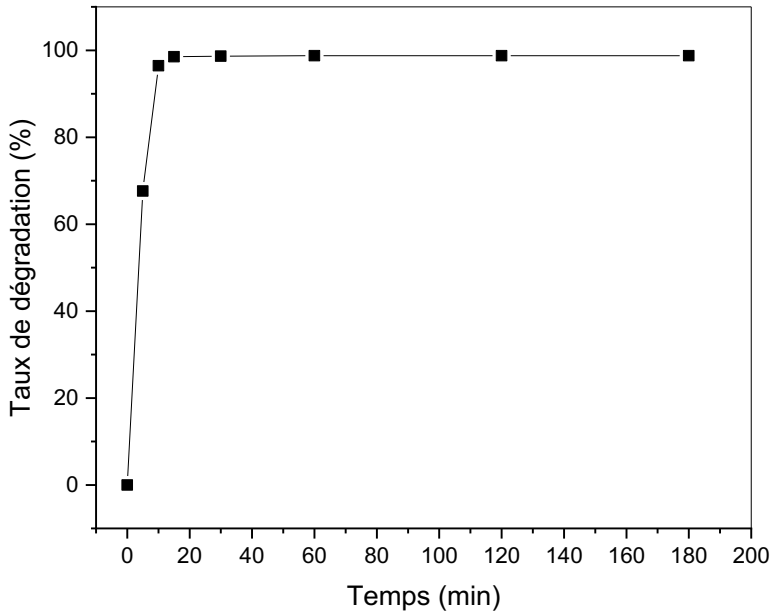

Figure 24. Degradation kinetics of RB-203 by direct photocatalysis under solar irradiation

Figure 25 shows a series of filter papers used to filter the samples collected in this experiment. A gradual decrease in the intensity of coloration of the deposits on the filters can be observed, indicating increasing degradation of the dye over time.

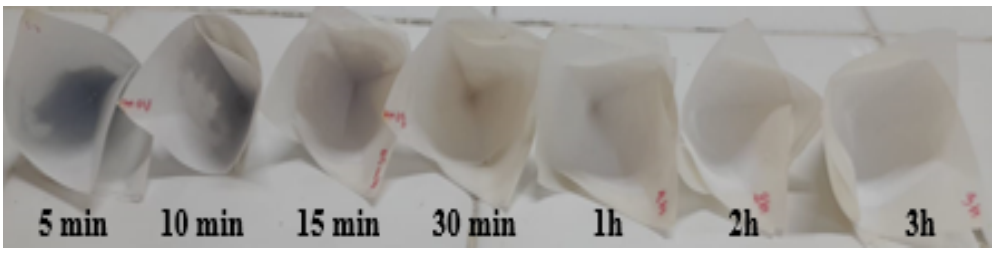

Figure 25. Evolution of filter paper coloration after photocatalysis of RB-203

The results of this photocatalysis are almost identical to those of the previous experiment, confirming that the first photocatalysis carried out after adsorption of the RB-203 dye by TiO2-25 works correctly.

Conclusion

The treatment of wastewater containing textile dyes poses a significant environmental challenge due to the complexity of the effluents and the diversity of chemical compounds present. This study explored several processes aimed at optimizing the purification efficiency of these waters. The results revealed that adsorption on TiO_2 is particularly effective, thanks to its high adsorption capacity and large specific surface area, especially for the removal of the dye RB-203. Kinetic analysis showed that adsorption equilibrium is reached in around 180 min. A study of the parameters influencing this adsorption determined that the optimum conditions for maximum discoloration rate are: a dye concentration of 40 mg/L, a quantity of TiO_2-P25 of 0.125 g, an acid pH of 3, a stirring speed of 300 rpm, and a temperature of 25 °C. Additionally, TiO_2-based photocatalysis has shown promising results in the degradation of RB-203 under solar irradiation, with TiO_2 recycling methods favoring cost reduction and process sustainability. In conclusion, this study proposes effective solutions for the treatment of wastewater containing textile dyes, with specific recommendations for the practical application of these techniques in industrial plants. Future prospects include optimizing treatment conditions and integrating these processes into broader water treatment systems for sustainable environmental management.

References

Ajmal, N., Saraswat, K., Bakht, M. A., Riadi, Y., Ahsan, M. J., & Noushad, M. (2019). Cost-effective and eco-friendly synthesis of titanium dioxide (TiO_2) nanoparticles using fruit's peel agro-waste extracts: characterization, in vitro antibacterial, antioxidant activities. *Green Chemistry Letters and Reviews*, *12*(3), 244-254. https://doi.org/10.1080/17518253.2019.1629641

Akartasse, N., Azzaoui, K., Mejdoubi, E., Hammouti, B., Elansari, L.L., Abou-salama, M., Aaddouz, M., Sabbahi, R., Rhazi, L., Siaj, M. (2022). Environmental-Friendly Adsorbent Composite Based on Hydroxyapatite/Hydroxypropyl Methyl- Cellulose for Removal of Cationic Dyes from an Aqueous Solution. Polymers, 14, 2147. https://doi.org/10.3390/polym14112147

Al-Taweel, S. S., & Saud, H. R. (2016). New route for synthesis of pure anatase TiO_2 nanoparticles via utrasound-assisted sol-gel method. *J. Chem. Pharm. Res,* 8(2), 620-626/

Ammari, Y., Elatmani, K., Qourzal, S., Bakas, I., Ejakouk, E., & Ait-Ichou, Y. (2016). (Kinetic study of the photocatalytic degradation of methylene blue dye in the presence of titanium dioxide (TiO_2), in aqueous suspension). *J. Mater. Environ*. Sci, 7(8). https://doi.org/10.1016/j.matpr.2019.08.142

Annan, E., Arkorful, G. K., Konadu, D. S., *et al*. (2021). Synthesis and Characterization of Hydroxyapatite-(HAP-) Clay Composites and Adsorption Studies on Methylene Blue for Water Treatment. *Journal of Chemistry*, 2021, 1–15. https://doi.org/10.1155/2021/3833737.

Assila, O., Miyah, Y., Nahali, L., El Badraoui, A., Nenov, V., El Khazzan, B., Zerrouq, F., Kherbeche, A. (2021). Copper-impregnated on natural material as promising catalysts for the wet hydrogen peroxide catalytic oxidation of Methyl Green. *Moroccan Journal of Chemistry* 9(1), 075–084. https://doi.org/10.48317/IMIST.PRSM/morjchem-v9i1.22256

Azzaoui, K., Mejdoubi, E., Lamhamdi, A., Zaoui, S., Berrabah, M., Elidrissi, A., Hammouti, B., et al. (2015) Structure and properties of hydroxyapatite/hydroxyethyl cellulose acetate composite films.

Carbohydrate Polymers. 115, 22, 170-176. https://doi.org/10.1016/j.carbpol.2014.08.089.

Azzaoui, K., Lamhamdi, A., Mejdoubi, E., et al. (2014). Synthesis and characterization of composite based on cellulose acetate and hydroxyapatite application to the absorption of harmful substances. *Carbohydrate Polymers,* 111, 41-46. https://doi.org/10.1016/j.carbpol.2014.04.058

Azzaoui, K., Mejdoubi, E., Lamhamdi, A., Hammouti, B., Akartasse, N., Berrabah, M. et al.(2016).Novel Tricomponenets composites Films From Polylactic Acid/ Hydroxyapatite/ Poly- Caprolactone Suitable For Biomedical Applications. *J. Mater. Environ. Sci*. 7 (3) ,761-769

Azzaoui K., Lamhamdi A., *et al*. (2014). Synthesis of hydroxyethylcellulose and hydroxyapatite composite for analysis of bisphenol A. *Arabian Journal of Chemical and Environmental Researches*. 1 , 41–48.

Burakov, A., Galunin, E., Burakova, I., Kucherova, A., Agarwal, S., Tkachev, A., & Gupta, V. (2018). Adsorption of heavy metals on conventional and nanostructured materials for wastewater treatment purposes: A review.. *Ecotoxicology and environmental safety*, 148, 702-712 . https://doi.org/10.1016/j.ecoenv.2017.11.034.

Dutta, S., Adhikary, S., Bhattacharya, S., Roy, D., Chatterjee, S., Chakraborty, A., ... & Rajak, P. (2024). Contamination of textile dyes in aquatic environment: Adverse impacts on aquatic ecosystem and human health, and its management using bioremediation. *Journal of Environmental Management*, *353*, 120103. https://doi.org/10.1016/j.jenvman.2024.120103

El Abdouni A., Bouhout S., Merimi I., *et al*. (2021), Physicochemical characterization of wastewater from the Al-Hoceima slaughterhouse in Morocco, *Caspian J. Environ. Sci.* 19(3), 423-429

El-Hafed, S., Bouslamti, R., Zerrouq, F., Kherbeche, A., Boualam, O., Nahali, L., ... & Agunaou, M. (2024). Optimization of CWPO for the Crystal violet and Methyl orange dyes degradation in the presence of copper-impregnated Moroccan clay catalysts. *Moroccan Journal of Chemistry*, *12*(3), 1097-1109. https://doi.org/10.48317/IMIST.PRSM/morjchem-v12i3.47474.

Elmoubarki, R., Mahjoubi, F., Tounsadi, H., Moustadraf, J., *et al*. (2015). Adsorption of textile dyes on raw and decanted Moroccan clays: Kinetics, equilibrium and thermodynamics. *Water Resources and Industry*, 9, 16-29. https://doi.org/10.1016/J.WRI.2014.11.001.

Giwa, A., Nkeonye, P. O., Bello, K. A., Kolawole, E. G., & Campos, A. O. (2012). Solar photocatalytic degradation of reactive yellow 81 and reactive violet 1 in aqueous solution containing semiconductor oxides. *International Journal of Applied,* 2(4), 90-105. https://doi.org/10.1016/j.mssp.2022.107261

Hamed, O., Lail, B.A., Deghles, A. et al. (2019). Synthesis of a cross-linked cellulose-based amine polymer and its application in wastewater purification. *Environ. Sci. Pollut. Res.* 26, 28080–28091. https://doi.org/10.1007/s11356-019-06001-4

Hasanpour, M., & Hatami, M. (2020). Application of three dimensional porous aerogels as adsorbent for removal of heavy metal ions from water/wastewater: A review study.. *Advances in colloid and interface science*, 284, 102247 . https://doi.org/10.1016/j.cis.2020.102247.

Hu, H., Lin, Y., & Hu, Y. (2020). Core-shell structured TiO2 as highly efficient visible light photocatalyst for dye degradation. *Catalysis Today*, 341, 90-95. https://doi.org/10.1016/J.CATTOD.2019.01.077.

Halim, W. (2021). Synthèse contrôlée par additifs latex de nanoparticules mésoporeuses à base de TiO_2: M (M= Pd, Ag, Cu, Ni...): caractérisation et applications en photocatalyse (Doctoral dissertation, Le Mans Université; Université Hassan II (Casablanca, Maroc)).

Ihmels, H. (2019). Dyes in modern organic chemistry. *Beilstein Journal of Organic Chemistry*, 15, 2798 - 2800. https://doi.org/10.3762/bjoc.15.272.

Jafari, S., Zhao, F., Zhao, D., Lahtinen, M., Bhatnagar, A., & Sillanpää, M. (2015). A comparative study for the removal of methylene blue dye by N and S modified TiO2 adsorbents. *Journal of Molecular Liquids*, 207, 90-98. https://doi.org/10.1016/J.MOLLIQ.2015.03.026.

Jallouli, N., Elghniji, K., Hentati, O., *et al.* (2016). UV and solar photo-degradation of naproxen: TiO_2 catalyst effect, reaction kinetics, products identification and toxicity assessment.. *Journal of hazardous materials*, 304, 329-36. https://doi.org/10.1016/j.jhazmat.2015.10.045.

Karim, A., Mounir, B., Hachkar, M., Bakasse, M., & Yaacoubi, A. (2009). Removal of Basic Red 46 dye from aqueous solution by adsorption onto Moroccan clay.. *Journal of hazardous materials*, 168 1, 304-9 . https://doi.org/10.1016/j.jhazmat.2009.02.028.

Kannan, K., Radhika, D., Vijayalakshmi, S., Sadasivuni, K. K., A. Ojiaku, A., & Verma, U. (2022). Facile fabrication of CuO nanoparticles via microwave-assisted method: photocatalytic, antimicrobial and anticancer enhancing performance. *International Journal of Environmental Analytical*

Chemistry, *102*(5), 1095-1108. https://doi.org/10.1080/03067319.2020.1733543
Kosmulski, M. (2016). Isoelectric points and points of zero charge of metal (hydr)oxides: 50years after Parks' review.. *Advances in colloid and interface science*, 238, 1-61 . https://doi.org/10.1016/j.cis.2016.10.005.
Kordouli, E., Bourikas, K., Lycourghiotis, A., & Kordulis, C. (2015). The mechanism of azo-dyes adsorption on the titanium dioxide surface and their photocatalytic degradation over samples with various anatase/rutile ratios. *Catalysis Today*, 252, 128-135. https://doi.org/10.1016/J.CATTOD.2014.09.010.
Lima, E., Sher, F., Guleria, A., Saeb, M., Anastopoulos, I., Tran, H., & Hosseini-Bandegharaei, A. (2020). Is one performing the treatment data of adsorption kinetics correctly?. *Journal of environmental chemical engineering*, 104813. https://doi.org/10.1016/j.jece.2020.104813.
Liu, S. (2015). Cooperative adsorption on solid surfaces.. *Journal of colloid and interface science*, 450, 224-238 . https://doi.org/10.1016/j.jcis.2015.03.013.
Marchant C. A., Briggs, K. A. and Long, A. (2008) In silico tools for sharing data and knowledge on toxicity and metabolism: Derek for windows, meteor, and vitic, *Toxicology Mechanisms and Methods*, 18(2–3), pp. 177–187. doi: 10.1080/15376510701857320.
Mészáros, R., Varga, I., & Gilányi, T. (2004). Adsorption of poly(ethyleneimine) on silica surfaces: effect of pH on the reversibility of adsorption.. *Langmuir : the ACS journal of surfaces and colloids*, 20 12, 5026-9 .https://doi.org/10.1021/LA049611L.
Moreira, N., Narciso-da-Rocha, C., Polo-López, M., Pastrana-Martínez, L., Faria, J., Manaia, C., Fernández-Ibáñez, P., Nunes, O., & Silva, A. (2018). Solar treatment (H2O2, TiO2-P25 and GO-TiO2 photocatalysis, photo-Fenton) of organic micropollutants, human pathogen indicators, antibiotic resistant bacteria and related genes in urban wastewater.. *Water research*, 135, 195-206 . https://doi.org/10.1016/j.watres.2018.01.064.
Mourid El H., Lakraimi M., Benaziz L., Cherkaoui M. (2021) Water reuse after removing a textile dye methyl orange using a recyclable hydrotalcite material, *Mor. J. Chem.* 9 N°1, 028-043, https://doi.org/10.48317/IMIST.PRSM/morjchem-v9i1.21114
Moyé, J., Picard-Lesteven, T., Zouhri, L., Amari, K., Hibti, M., & Benkaddour, A. (2017). Groundwater assessment and environmental impact in the abandoned mine of Kettara (Morocco).. *Environmental pollution*, 231 Pt 1, 899-907 . https://doi.org/10.1016/j.envpol.2017.07.044.
Nasiruddin K. M. and Sawar A. (2007) Determination of point of charge of natural and treated adsorbents, Surface Review and Letters, 14(3), 461-469. https://doi.org/10.1142/S0218625X07009517.
Srinivasan, M., Venkatesan, M., Arumugam, V., Natesan, G., Saravanan, N., Murugesan, S., ... & Pugazhendhi, A. (2019). Green synthesis and characterization of titanium dioxide nanoparticles (TiO2 NPs) using Sesbania grandiflora and evaluation of toxicity in zebrafish embryos. *Process Biochemistry,* 80, 197-202. https://doi.org/10.1016/j.procbio.2019.02.010
Hamed, O., Lail, B.A., Deghles, A. et al. (2019). Synthesis of a cross-linked cellulose-based amine polymer and its application in wastewater purification. *Environ Sci Pollut Res.* 26, 28080–28091. https://doi.org/10.1007/s11356-019-06001-4
Saidi, N., Azzaoui, K., Ramdani, M., Mejdoubi, E., Jaradat, N., Jodeh, S., Hammouti, B., Sabbahi, R., Lamhamdi, A. (2022). Design of Nanohydroxyapatite/ Pectin Composite from Opuntia Ficus-Indica Cladodes for the Management of Microbial Infections. *Polymers*, 14, 4446. https://doi.org/10.3390/polym14204446
Tkaczyk, M. (2020). origin, differences and meaning in modern plant pathology. *Folia Forestalia Polonica*, *62*(3), 227-232.
Vetrivel V., Rajendran K., *et al*. (2015). Synthesis and characterization of pure titanium dioxide nanoparticles by sol-gel method. *Int. J. ChemTech* Res, 7(3), 1090-1097. doi:10.15680/IJIRSET.2014.0308020.
Wozniak, M., Witkowski, B., Gierczak, T., & Biesaga, M. (2023). First Dye Identification Analyses Conducted on Textiles from Old Dongola (Sudan, 17th-18th centuries CE). *Archaeometry*. https://doi.org/10.1111/arcm.12930.